

Data Repository Item: additional study site, sample and analytical information

1. Sampling of CC28 and stable isotope analysis

Stable isotope analyses were performed using an Analytical Precision AP2003 continuous-flow isotope-ratio mass spectrometer. Precision based on replicates of the SUERC laboratory standard (Carrara Marble) was 0.07‰ for $\delta^{13}\text{C}$ and 0.12‰ for $\delta^{18}\text{O}$ ($n = 122$). The sample powders were micromilled at 100 μm increments using a lathe. Although milling was conducted over a short distance (3 mm) perpendicular to the growth axis (i.e. parallel to the laminations), cross-sampling is inevitable due to microscale variations in layer geometry (Fairchild et al. 2006). Consequently, we estimate that the true sampling precision is $\pm 200 \mu\text{m}$ from the midpoint of a given 100 μm increment.

The stalagmite was fed by a drip point whose position apparently shifted during its growth. As a consequence, milling was performed along three transects (Transects 1-3, Figure DR1). We ensured that each traverse overlapped so that pattern matching could be used to splice together the three separate sections into a single composite series. The $\delta^{13}\text{C}$ proved to be the most satisfactory for this purpose: their values are better resolved analytically and possess greater temporal variation than $\delta^{18}\text{O}$. The $\delta^{13}\text{C}$ isotopic data for the overlapping segments are shown in Figure DR2. The x-error bars represent the 400 μm sampling error envelope (i.e. $\pm 200 \mu\text{m}$ either side of the sampling midpoint), whilst the y-error bars represent the magnitude of maximum isotopic variations along growth layers in previously studied Corchia stalagmites ($\sim 0.5\%$).

The $\delta^{13}\text{C}$ values for the upper transition (Transect 1 – Transect 2 boundary; top panel of Figure DR2) are in excellent agreement with one another. A minor dilemma was the discrepancy in $\delta^{13}\text{C}$ values at the lower transition (Transect 2 – Transect 3 boundary; bottom panel of Figure DR2). This transition marks the time when the drip point shifted significantly. The consequent change in growth orientation is clearly marked by the bench-like feature on the right edge of the stalagmite (Figure DR1). It is possible that the calcite in the upper few millimeters of Transect 3 was enriched in ^{13}C due to Rayleigh-distillation processes (Bar-Matthews et al. 1996; Mickler et al. 2006), although the $\delta^{18}\text{O}$ data do not display any such systematic offset (mean of basal Transect 2 $\delta^{18}\text{O} = 4.00 \pm 0.10\%$; mean of upper Transect 3 $\delta^{18}\text{O} = 4.04 \pm 0.16\%$). We adopted a conservative approach of employing the lower-amplitude values of Transect 2 in the composite series.

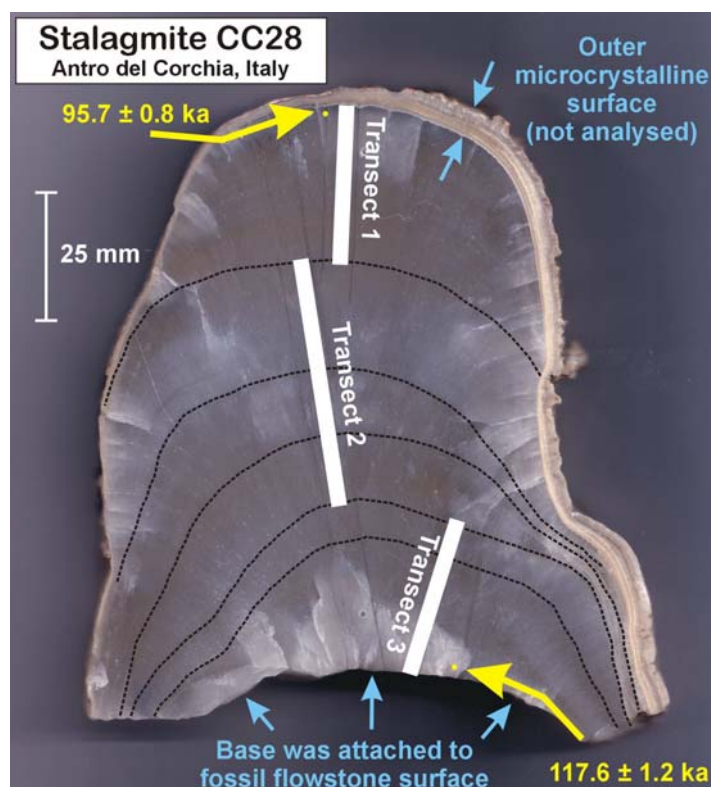


Figure DR1: Polished section of CC28 showing the three milled transects and top and basal ages (ka).

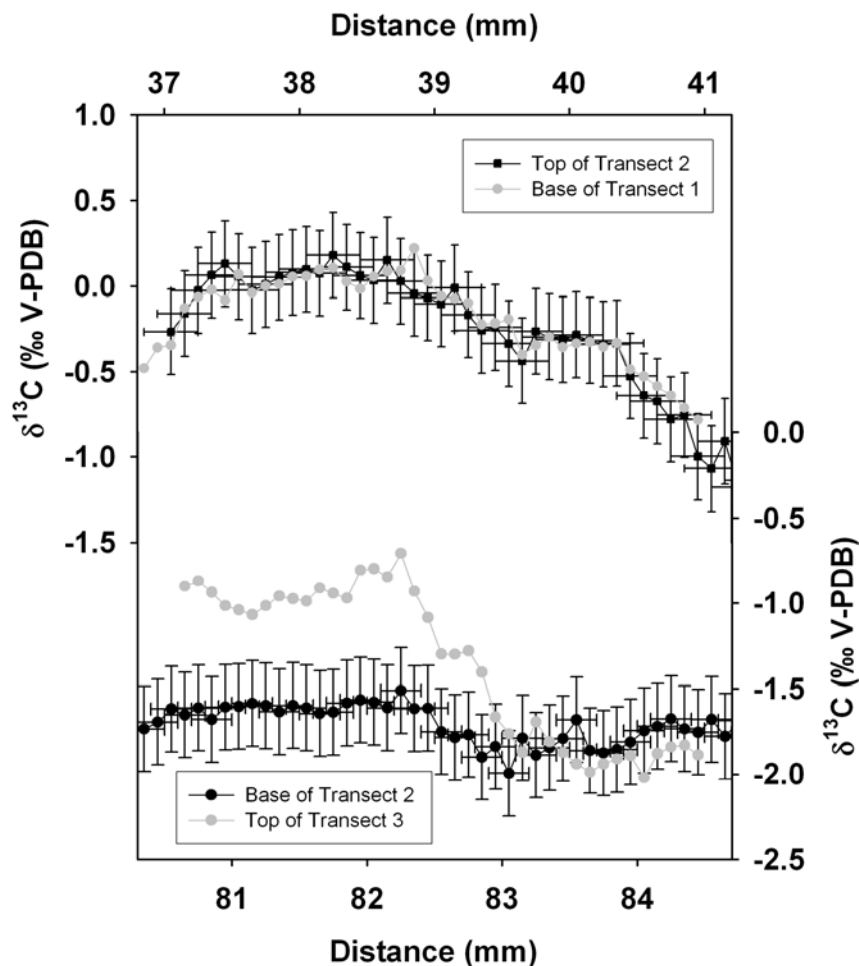


Figure DR2: $\delta^{13}\text{C}$ values for overlapping sections of the three milling traverses.

The isotopic composition of a series of samples collected consecutively along three separate traverses was measured to test for evidence of kinetic fractionation. These analyses were performed using a ThermoFinnigan Gas Bench and a Finnigan MAT 252 stable isotope-ratio mass spectrometer operating in continuous flow mode (Drysdale et al. 2006). Reproducibility was 0.07‰ for $\delta^{13}\text{C}$ and 0.13‰ for $\delta^{18}\text{O}$. Previous studies of Corchia stalagmites (Drysdale et al. 2004; 2005) have shown that calcite is deposited at or close to isotopic equilibrium except immediately adjacent to hiatuses, where evaporative effects are likely. This trend is confirmed in CC28, with values exhibiting no positive correlation. Furthermore, the overall scatter of data points shows no significant covariation (Figure DR3). However, there are intervals during which $\delta^{13}\text{C}$ and $\delta^{18}\text{O}$ covary, as shown in Figure DR4. There is an entirely plausible paleoclimatic explanation for this, as discussed in the article. Indeed, periodic covariance between $\delta^{13}\text{C}$ and $\delta^{18}\text{O}$ seems too be relatively common in speleothem studies (Mickler et al. 2006). Figure DR5 shows time series from six well-known speleothem studies where stable isotopes have been used as the main paleoclimate proxy. We compiled 30-point running correlation coefficients (r) from the $\delta^{13}\text{C}$ and $\delta^{18}\text{O}$ data in these studies to highlight periods where statistically significant correlations occur. Perfectly reasonable paleoclimatic interpretations have been proposed for the isotopic patterns observed in these studies.

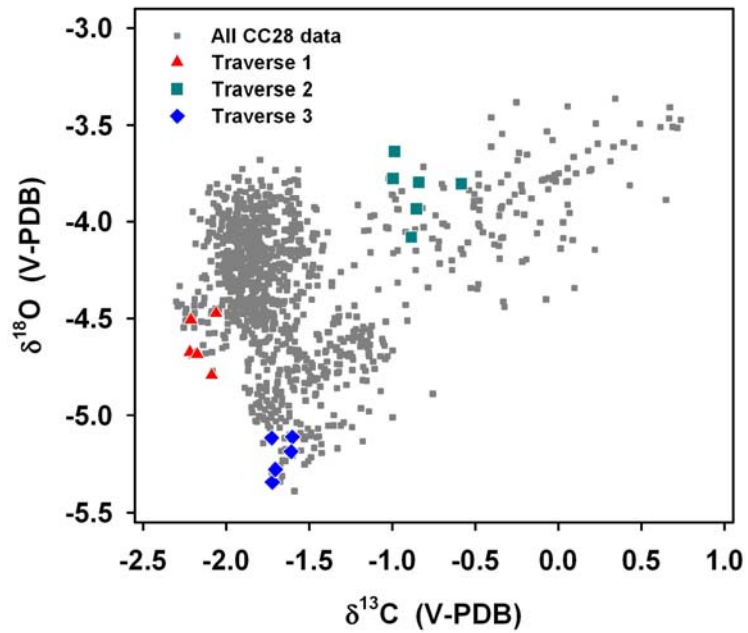


Figure DR3: Bivariate plot of $\delta^{18}\text{O}$ and $\delta^{13}\text{C}$ data derived from traverse samples (coloured symbols). The lack of positive correlation suggests the calcite was not affected by kinetic fractionation. Also shown is the bivariate plot of main axis isotope values.

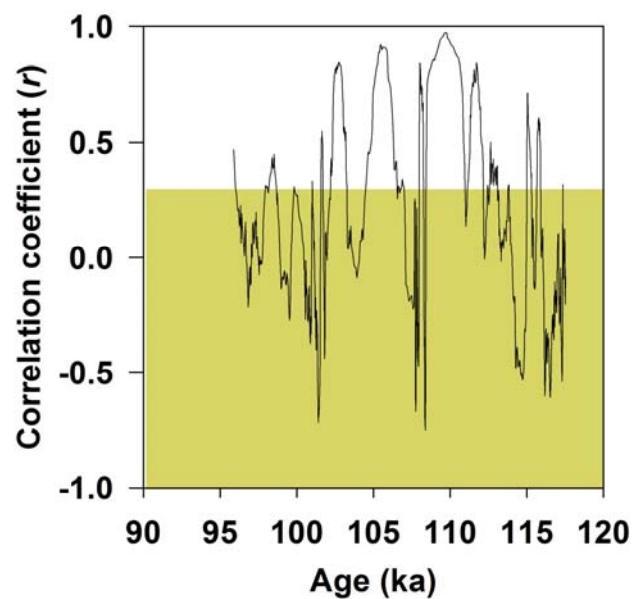


Figure DR4: Running 30-point correlation coefficient (r) for CC28. The unshaded zone is where the r value becomes statistically significant, i.e. critical value of r is 0.36 for $p < 0.05$, $n = 30$, $df = 28$.

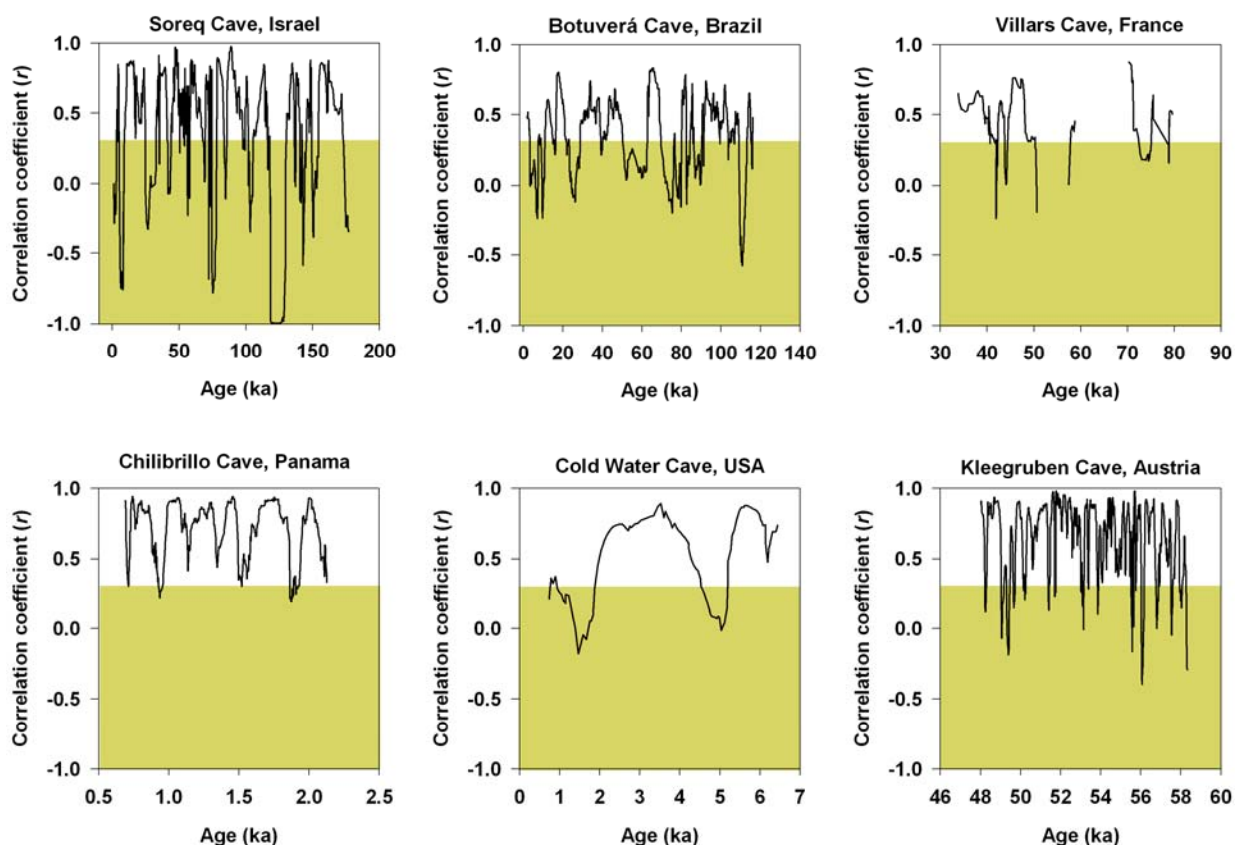


Figure DR5: Running 30-point correlation coefficients for six speleothem time series (Soreq Cave: Bar-Matthews et al. 2000, 2003; Botuvera Cave: Cruz et al. 2005; Villars Cave: Genty et al. 2003; Chilibrillo Cave: Lachniet et al. 2004; Cold Water Cave: Denniston et al. 1999; Kleegruben Cave: Spötl et al. 2006). The unshaded zone of each series is the region where statistically significant correlations prevail.

2. Age data and depth-age model

All age data are shown in Table DR1. The columns “ $(^{234}\text{U}/^{238}\text{U})_{\text{act}}$ ” and “ $(^{230}\text{Th}/^{238}\text{U})_{\text{act}}$ ” are activity ratios obtained by normalizing measured atomic ratios to the long-term average of those measured from a solution of the HU-1 equilibrium standard – see Hellstrom (2003) for a complete description of the MC-ICP-MS method used. Ages and “ $(^{234}\text{U}/^{238}\text{U})_{\text{initial}}$ ” values are calculated using Isoplot/Ex 2.49n, using decay constants of 9.195×10^{-6} (^{230}Th) and 2.835×10^{-6} (^{234}U). The position of tip and basal age data points is shown in Figure DR1. The depth position of samples for the remaining U/Th ages, derived from powders leftover from the stable isotope analyses, is shown in Table DR1. The depth-age model used to construct the stable isotope time-series is shown in Figure DR6, whilst the derived age-for-age-uncertainty model is shown in Figure DR7. A discussion of the techniques for generating this and the depth-age model is provided in the supplementary information for Drysdale et al. (2005).

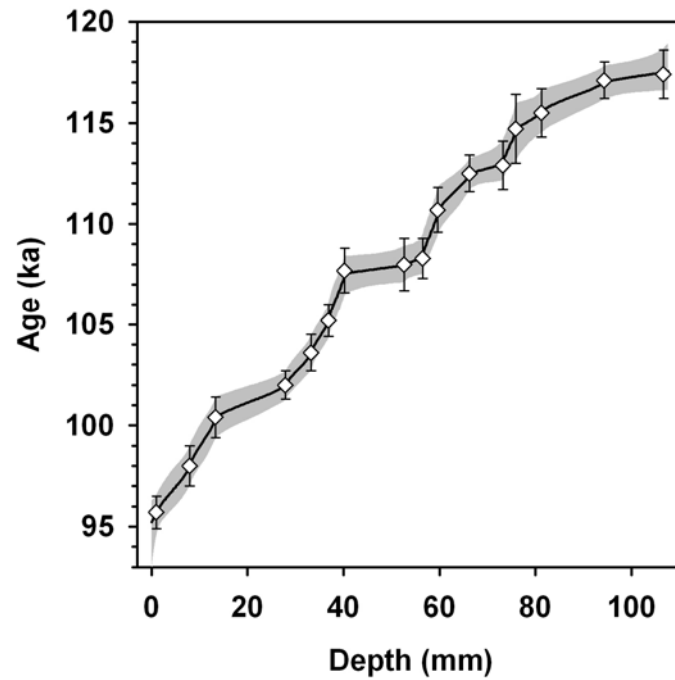


Figure DR6: Depth-age model for CC28 based on data shown in Table DR1.

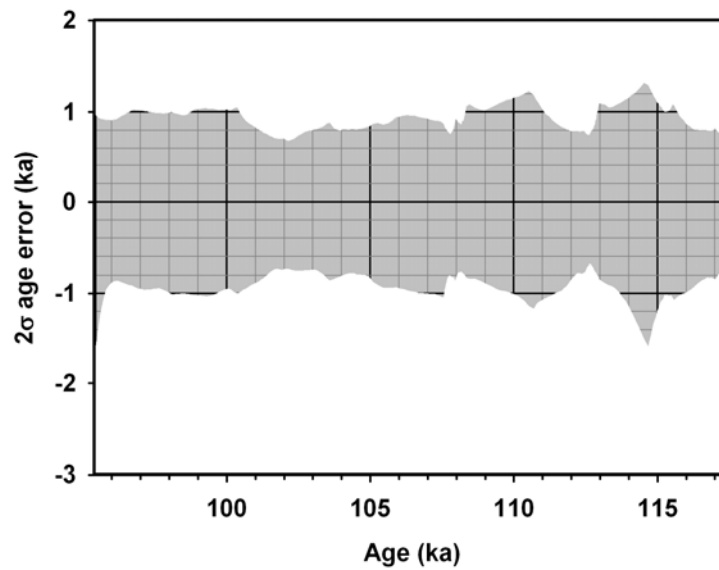


Figure DR7: Age-for-age-uncertainty model for CC28. This provides estimates of the 2σ uncertainty for each age increment through the time series.

Table DR1: Age and depth data for stalagmite CC28. The numbers in round brackets are 95% uncertainties. Isotope data are expressed as activity ratios, the 95% uncertainties for which include allowances for external standard reproducibility and spike calibration uncertainty, although uncertainty in decay constants is not propagated. [$^{230}\text{Th}/^{238}\text{U}$] is determined using a mixed spike calibrated against a solution of HU-1 - see Hellstrom (2003) for a detailed description of the method and results of standard analyses. Age is calculated using the standard U-Th age equation, and employing decay constants of 9.195×10^{-6} and 2.835×10^{-6} for ^{230}Th and ^{234}U respectively. The age and initial $^{234}\text{U}/^{238}\text{U}$ activity ratios ($[\text{234}/\text{238}]_i$) have been corrected for detrital Th assuming an initial $^{230}\text{Th}/^{232}\text{Th}$ activity ratio of 1 ± 1 and propagating its uncertainty via an additional term in the standard U-Th age equation. [$^{234}\text{U}/^{238}\text{U}$]_i is calculated using [$^{234}\text{U}/^{238}\text{U}$] and the corrected age.

Sample	Depth mm ($\pm 2\sigma$)	Mass (mg)	U ($\mu\text{g g}^{-1}$)	[$^{230}\text{Th}/^{238}\text{U}$] ($\pm 2\sigma$)	[$^{234}\text{U}/^{238}\text{U}$] ($\pm 2\sigma$)	[$^{232}\text{Th}/^{238}\text{U}$] $\times 10^3$ ($\pm 2\sigma$)	Age ka ($\pm 2\sigma$)	[$^{234}\text{U}/^{238}\text{U}$] _i ($\pm 2\sigma$)
CC28-2	1.05 (1.00)	5.4	2.20	0.4135 (0.0018)	0.7396 (0.0018)	0.0728 (0.0018)	95.7 (0.8)	0.659 (0.003)
CC28-81	7.95 (0.20)	3.3	2.59	0.4190 (0.0024)	0.7392 (0.0021)	0.0532 (0.0019)	98.0 (1.0)	0.656 (0.003)
CC28-135	13.35 (0.20)	2.1	2.95	0.4253 (0.0022)	0.7400 (0.0022)	0.0625 (0.0031)	100.4 (1.0)	0.654 (0.004)
CC28-281	27.95 (0.20)	2.9	3.22	0.4315 (0.0015)	0.7434 (0.0017)	0.0260 (0.0017)	102.0 (0.7)	0.657 (0.003)
CC28-334	33.25 (0.20)	3.1	3.16	0.4392 (0.0019)	0.7491 (0.0016)	0.1619 (0.0013)	103.6 (0.9)	0.663 (0.003)
CC28-439-440	36.90 (0.30)	2.8	4.19	0.4413 (0.0019)	0.7467 (0.0015)	0.1214 (0.0011)	105.2 (0.8)	0.659 (0.002)
CC28-473	40.25 (0.20)	1.7	3.29	0.4436 (0.0022)	0.7422 (0.0021)	0.0423 (0.0041)	107.7 (1.1)	0.650 (0.003)
CC28-597	52.65 (0.20)	3.5	2.50	0.4446 (0.0028)	0.7425 (0.0018)	0.0192 (0.0021)	108.0 (1.3)	0.650 (0.003)
CC28-635	56.45 (0.20)	2.2	2.73	0.4469 (0.0020)	0.7449 (0.0023)	0.0291 (0.0027)	108.3 (1.0)	0.653 (0.004)
CC28-667	59.65 (0.20)	2.4	2.06	0.4542 (0.0024)	0.7477 (0.0018)	0.0286 (0.0020)	110.7 (1.1)	0.655 (0.003)
CC28-732-734	66.25 (0.40)	6.6	3.90	0.4590 (0.0017)	0.7488 (0.0014)	0.0118 (0.0009)	112.5 (0.9)	0.654 (0.002)
CC28-801-803	73.15 (0.40)	2.2	3.07	0.4608 (0.0024)	0.7500 (0.0019)	0.0197 (0.0026)	112.9 (1.2)	0.656 (0.003)
CC28-829	75.85 (0.20)	1.8	2.72	0.4626 (0.0035)	0.7473 (0.0027)	0.0286 (0.0035)	114.7 (1.7)	0.650 (0.005)
CC28-883	81.25 (0.20)	1.8	3.00	0.4659 (0.0023)	0.7496 (0.0018)	0.0343 (0.0050)	115.5 (1.2)	0.653 (0.003)
CC28-1144	94.35 (0.20)	4.2	3.79	0.4704 (0.0017)	0.7513 (0.0016)	0.0155 (0.0009)	117.1 (0.9)	0.653 (0.003)
CC28-1020	106.65 (1.00)	10.5	4.21	0.4738 (0.0024)	0.7547 (0.0017)	0.0781 (0.0018)	117.4 (1.2)	0.658 (0.003)

3. Carbon isotope trends in Corchia speleothems during interglacial periods

Figure DR8 shows $\delta^{13}\text{C}$ and $\delta^{18}\text{O}$ time series for three interglacial phases (Marine Isotope Stages 9, 5 and 1 – grey bars) from Antro del Corchia stalagmites. The consistency of the progressive shift from higher to lower values through each glacial-interglacial transition is evident, as is the tendency for the lightest $\delta^{13}\text{C}$ values, presumed to represent the greatest input of biogenic CO_2 (reflecting the mature phase of soil development), to occur well into each interglacial. Indeed, the $\delta^{13}\text{C}$ values over the first 10,000 years of each interglacial are remarkably similar, in spite of the data coming from independent speleothems. This suggests that a consistent process occurs through each interglacial following a given glacial termination. We suggest that a considerable time lag exists for post-glacial soils to develop. The terrain above the cave is very steep. Today, the soil mantle is highly discontinuous, being confined to shallow, joint-controlled dissolution features and larger depressions where periglacial material (probably formed during glacial periods) has accumulated. The amount of bare rock surface is high. The ground surface has a sparse vegetation cover of grasses and occasional low shrubs. Elsewhere in the region the treeline extends at least several hundred meters above the summit altitude of Monte Corchia, suggesting that today's low vegetation cover on Monte Corchia is controlled primarily by the paucity of soil and the abundant bare rock surfaces. The high rainfall ($>3000 \text{ mm a}^{-1}$), steep terrain and high purity of the carbonate bedrock clearly conspire to inhibit soil development. The consistency of the $\delta^{13}\text{C}$ values for three interglacials suggests that the pattern we see today has probably persisted for at least the last 300-400 ka. The CC1 data are from Drysdale et al. (2004). The $\delta^{13}\text{C}$ measurements for CC5 were made on the same powders as for $\delta^{18}\text{O}$ reported in Drysdale et al. (2005). The isotope data for CC26 are unpublished.

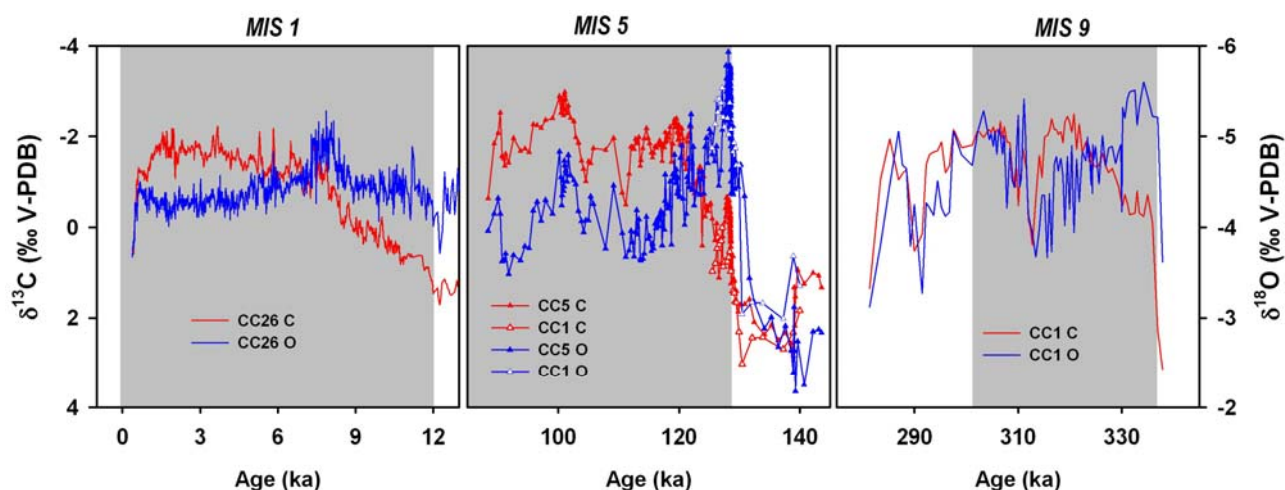


Figure DR8: $\delta^{13}\text{C}$ and $\delta^{18}\text{O}$ trends during the progression of three interglacials.

4. Site recharge

In spite of the deep position of the sampling chamber within the cave system, there are several lines of evidence to suggest that there is not a significant time lag between the onset of a climatic perturbation and its incorporation into the Corchia speleothems. Firstly, tritium measurements performed on samples from two drip sites (one from the speleothem sample chamber and another from a nearby point at a similar elevation) indicate recharge rainfall from the 1950s (Doveri et al. 2005). Secondly, our previously published work describing the timing for the onset of the Last Interglacial at Corchia Cave (Drysdale et al. 2005) is in excellent agreement with the Eastern Mediterranean (Bar-Matthews et al. 2003) and Chinese (Yuan et al. 2004) speleothem records. Thirdly, a Holocene speleothem from the same chamber in Corchia (CC26 - the results of which are currently 'in review') show that the timing of the Sapropel 1 event is in very good agreement (within a couple of hundred years) with the Soreq Cave record (Bar-Matthews et al. 1999). Together, this suggests that recharge rainfall is transmitted to the sample chamber relatively rapidly, and that the age discrepancy between CC28 and other proxies for the cold events referred to in the article are not due to water residence-time factors.

5. Depth-age model for the age data of Cruz et al. (2005)

We applied the same Bayesian Monte Carlo technique as mentioned in section 2 above to the raw depth-age data of Cruz et al. (2005) to produce an age-versus-age-uncertainty plot from which we quantified the age uncertainties associated with the $\delta^{18}\text{O}$ time series of BT2 (Figure DR9). The two excursions highlighted by the gray shading appear to correspond to events C24 and C23 in CC28 and the North Atlantic marine record. Superimposed over the BT2 age-versus-age-uncertainty output is the equivalent output for CC28. The uncertainties through these events in BT2 range average 2.5 ka, whereas the corresponding uncertainties for CC28 average 0.9 ka.

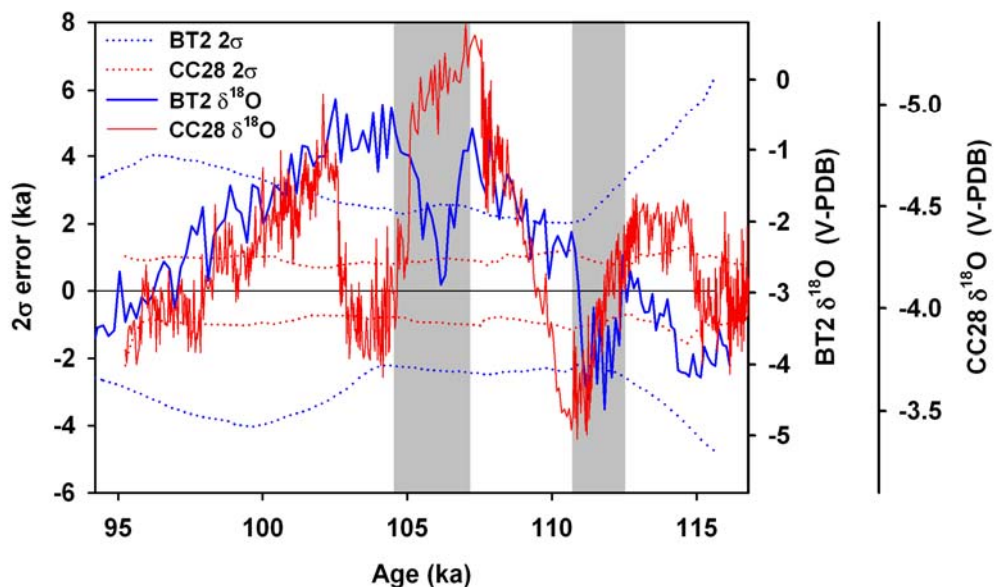


Figure DR9: $\delta^{18}\text{O}$ time series (solid lines) and age vs age uncertainty plots (dotted lines) of BT2 Cruz et al. (2005) (blue) and CC28 (red). Lower levels of age uncertainty are evident for the CC28 series. The shaded zones represent the intervals from BT2 from which the error values quoted in the text were derived.

ADDITIONAL REFERENCES USED HERE THAT ARE NOT CITED IN THE ARTICLE

- Bar-Matthews M., Ayalon, A., Matthews, A., Sass, E., and Halicz, L. 1996, Carbon and oxygen isotope study of the active water carbonate system in a karstic Mediterranean cave: Implications for palaeoclimate research in semiarid regions: *Geochimica et Cosmochimica Acta*, v. 60, p. 337–347.
- Bar-Matthews, M., Ayalon, A., Kaufman, A., and Wasserburg, G.J., 1999, The Eastern Mediterranean palaeoclimate as a reflection of regional events: Soreq cave, Israel: *Earth and Planetary Science Letters*, v. 166, p. 85–95.
- Bar-Matthews, M., Ayalon, A., and Kaufman, A., 2000, Timing and hydrological conditions of Sapropel events in the Eastern Mediterranean, as evident from speleothems, Soreq cave, Israel: *Chemical Geology*, v. 169, p. 145–156
- Doveri, M., Leone, G., Mussi, M., and Zanchetta, G., 2005, Composizione isotopica di acque ipogee dell'Antro del Corchia, Alpi Apuane, Toscana Nord-Occidentale: *Istituto Italiano di Speleologia Memoria*, v. 18, suppl. 2, p.119-132.
- Drysdale, R., Zanchetta, G., Hellstrom, J., Maas, R., Fallick, A., Cartwright, I., Piccini, L. and Pickett, M., 2006, Late Holocene drought responsible for the collapse of Old World civilizations is recorded in an Italian cave flowstone: *Geology*, v. 34, p. 101-104.
- Fairchild, I., Smith, C.L., Baker, A., Fuller, L., Spötl, C., Matthey, D., McDermott, F., and E.I.M.F., 2006, Modification and preservation of environmental signals in speleothems: *Earth Science Reviews*, v. 75, p. 105-153.
- Lachniet, M.S., Burns, S.J., Piperno, D.R., Asmerom, Y., Polyak, V.J., Moy, C.M., and Christenson, K., 2004b, A 1500-year El Niño/Southern Oscillation and rainfall history for the Isthmus of Panama from speleothem calcite: *Journal of Geophysical Research—Atmospheres*, v. 109, D20117, doi: 10.1029/2004JD004694.
- Mickler, P.J., Stern, L.A., and Banner, J.L. 2006, Large kinetic isotope effects in modern speleothems: *Geological Society of America Bulletin*, v. 118, p. 65-81.